IEEE Access
Multidisciplinary | Rapid Review | Open Access Journal

Received 24 June 2022, accepted 16 July 2022, date of publication 8 August 2022, date of current version 5 October 2022.

Digital Object Identifier 10.1109/ACCESS.2022.3197178

RESEARCH ARTICLE

3D Printed Active Origami Dielectrics for Frequency Tunable Antennas Through Mechanical Actuation

YINGWEI WU[1], ANDREA VALLECCHI[2], (Member, IEEE), YUNFANG YANG[2], ZHONG YOU[2], EKATERINA SHAMONINA[2], (Member, IEEE), CHRISTOPHER J. STEVENS[2], (Member, IEEE), AND PATRICK S. GRANT[3]

[1]TWI Technology Centre, Rotherham S60 5TZ, U.K.
[2]Department of Engineering Science, University of Oxford, Oxford OX1 3PJ, U.K.
[3]Department of Materials, University of Oxford, Oxford OX1 3PJ, U.K.

Corresponding author: Yingwei Wu (yingwei.wu@twi.co.uk)

This work was supported in part by the U.K. Engineering and Physical Sciences Research Council under Grant EP/P005578/1 and Grant EP/N010493/1, and in part by Kennametal Inc.

ABSTRACT We investigate using a reconfigurable metamaterial structure based on high permittivity dielectric elements in a flexible origami framework to control the electromagnetic response of a suspended patch antenna. Origami-inspired dielectric structures are fabricated by additive manufacturing of origami elements using an ABS-30 vol% $BaTiO_3$ filament (permittivity ∼11). The printed millimeter-scale elements are then assembled into an origami structure using flexible polymer hinges. Alternatively, dielectric origami structures are also achieved using a flexible, polymer-only origami lattice pre-fabricated by stereolithography into which shaped high dielectric elements (permittivity ∼18) of ABS-60 vol% $CaTiO_3$, manufactured by field assisted sintering, are inserted. The various dielectric origami designs are inserted into the air gap between a suspended patch antenna and a ground plane, designed to operate at a resonant frequency of 1 GHz. The presence of the dielectric origami modifies the antenna resonant frequency and tunablity is then achieved through different configurations of the dielectric origami, actuated by hand or mechanically. Tunability arises because varying the configuration, and overall density, of the dielectric origami varies its effective permittivity and thus the patch resonant frequency. The dielectric origami structures provide a tunable range up to ∼14%, in good agreement with numerical simulations. Simulations are also used to show how broader tunability could be achieved easily, for example, by optimizing the size of the dielectric elements. Overall, the results using these preliminary dielectric origami structures, enabled by combining advanced manufacturing techniques, suggest that the approach offers a wide design space with the potential to realise novel antenna functionality and flexibility.

INDEX TERMS Additive manufacturing, dielectric substrates, effective permittivity, origami dielectrics, patch antennas.

I. INTRODUCTION

Continuous advancement of wireless communication [1], [2] and the growing number of applications requiring wireless connectivity have boosted the demand for compact wireless systems capable of multi-frequency and multi-band operation. To meet the increasingly stringent requirements on bandwidth and limited device space, it has become crucial for antennas to have wideband frequency reconfigurability capabilities [3], [4]. Achieving reconfigurability in an antenna, for example, by adding the capability of modifying its operating frequency, bandwidth, and/or radiation properties dynamically, can significantly improve the system performance and reduce the number of antennas needed to meet certain communication requirements [5].

Common methods to achieve the reconfigurability of antennas can be grouped into three categories: electronic devices, tunable materials, and mechanical actuation [6].

The associate editor coordinating the review of this manuscript and approving it for publication was Shah Nawaz Burokur.

Examples from electronic devices include pin diodes [7], varactor diodes [8], microelectromechanical switches (MEMS) [9], or even a combination of these [10], where antenna radiation characteristics are electrically modified through switching or tuning elements.

However, these methods present a number of drawbacks and limitations. The operation of active devices requires bias voltages or currents to realize the desired variation of electrical parameters or properties; the biasing and control circuits can considerably increase the complexity of the system, and introduce additional losses, therefore increasing power consumption. Moreover, due to the non-linear nature of active devices, spurious frequency components can be produced. Another issue is that the power handling of these reconfigurable antennas is limited by the risk of an electrical breakdown of the active components, precluding their use in high-power applications.

Tunable materials such as ferroeletrics, ferrites, liquid crystal and semiconductors can be contrived with electrical properties that can be controlled by the application of external bias (e.g. heat, electric or magnetic field, optical radiation, etc). However, they generally require high bias voltages or high DC power consumption and show unwanted thermal sensitivity. An overivew of tunable materials can be found in [6].

Recently, mechanical actuation using microfluidics to reconfigure tunable antennas was shown to provide significant performance advantages compared with conventional reconfigurable antennas, including: improved linearity and higher power handling, together with the possibility of achieving continuous tuning and lower overall power losses/consumption. In these antennas the microfluidically controlled loads, acting as either a shorting, loading, or main radiating element, are moved using different actuation mechanisms. In the shorting based approach, liquid metal is used as a microfluidically controlled shorting switch. This technique has been used to implement frequency tunable slot [11] and patch antennas [12]. In the loading based approach, microfluidically controlled loads are placed on top of the radiating antenna to alter the electromagnetic fields, thereby changing the resonating properties. The reactive loads can either be liquid metals [13] or liquid dielectrics, such as acetone [14] and de-ionized water [15], [16]. However, there are challenges to achieving practical fluidic antennas. The mechanical pumping method that is required to actuate reconfigurability generally has a slow tuning speed [12]. In addition, the overall size of the antenna system, including the associated feeds, liquid containers, pumping and control system, may be bulky, and the robustness of such antennas is unproven. Finally, cost-effective fabrication on a large scale and the design of packaging and feeding of the antenna are yet to be resolved [17].

An alternative approach to accomplish reconfigurability/tunability without resorting to electronic components is by using transformable origami-inspired structures that leverage cutting and folding techniques [18], [19]. This approach has the advantage of enabling the creation of deployable structures with continuous-state reconfigurability, as opposed to discrete states, and large size ratios from folded to unfolded states [20], [21], [22]. Moreover, the actuation mechanisms for changing the shape of the origami structures can be easily implemented directly onto an antenna. Typical origami structures use folding of creases or at hinges to change their configuration. The most common applications of origami structures are for mechanical manipulation. For example, a twisted tower soft robot inspired by origami structures has been fabricated using a flexible material for the creases and a rigid material for the facets to demonstrate the ability to grasp objects robustly [23]. A similar concept can be applied to design deployable and foldable shape-changing origami-based antennas. For example, researchers have demonstrated the use of creased paper to create foldable origami structures to tune the operating frequency of spring and accordion antennas printed on them by changing the height of the structure [24], [25], [26]. However, those origami structures lack accurate and robust control over the reconfiguration states, and are somewhat delicate. Other origami antennas have been implemented using shape memory polymers (SMPs) as substrates [27], [28], which are more robust, but exhibit limited adhesion to conductors that are also required in the design.

To achieve the desired foldability repeatedly, and without bending or additional connecting elements, additively manufactured or 3D printed origami structures are beginning to emerge. Additive manufacturing (AM) has garnered significant attention due to its geometric and design flexibility, and the potential to reduce manufacturing steps. There are many AM technologies [29], such as fused filament fabrication (FFF), stereolithography (SLA), direct ink writing, and selective laser melting, to process feedstock materials that maybe in the form of filaments [30], resins [31], liquid solutions [32], or powders [33] to fabricate a three dimensional complex object. Among the variety of AM techniques, FFF and SLA are the two most promising manufacturing techniques for antenna applications [34], [35], due to their relative simplicity and wide availability of printable materials. In FFF, a thermoplastic filament is fed through a heated chamber and then into a nozzle of typically $\sim$0.4 mm diameter. The chamber heats the filament above its glass transition temperature and then extrudes the molten filament through the nozzle onto a heated print bed. Either the print head or the print bed moves in the x–y plane to print a layer. After a layer of material is printed, the print bed is lowered one layer thickness (typically $\sim$100 μm) to allow the next layer to be deposited. The process repeats until the part is complete. The main restrictions of FFF for antenna manufacturing are the limited thermoplastic filament choices, especially where high permittivity or permeability is needed, and the tendency for inter-layer roughness (often $\gg$10 μm) [36]. In SLA, a laser is used as a power source to cure selectively a photosensitive resin in a layer by layer fashion. The laser spot is $\sim$140 μm in diameter, and the layer thickness is $\sim$25 μm, giving reduced

surface roughness compared with FFF. However, with SLA it is difficult to print multi-material devices using a single resin tank without contamination from different materials.

A method to directly 3D print origami assemblages by introducing hinge-panel elements and a photocurable elastomer system for the hinges to ensure foldability and repeatability, was proposed in [37], [38]. Moreover, both FFF and SLA have been used to develop foldable antennas. For example, in [39] a cross-shaped structure was created with FFF from VeroWhite plastic (relative permittivity $\epsilon_r \simeq 3$) that could be folded to a cuboid with antennas printed directly on the cube surface [39]. SLA has been used to print a bow-tie antenna inspired from origami fan with an elastic resin ($\epsilon_r = 2.7$) and then the structure metallized using liquid metal alloy to facilitate folding [40]. As another example, a bow-tie antenna inspired by an origami fan has been realized by SLA with an elastic resin ($\epsilon_r = 2.7$), followed by metallizing with liquid metal alloy [40]. A detailed summary of recent advances in origami antennas and their construction from microwaves to to millimetre waves has been recently presented in [41]. Generally, these 3D printed origami radiating structures show a limited tuning range (less than 15%) due to the limited permittivity changes and no demonstration of mechanical actuation has been reported. Recent work has also addressed measuring the permittivity of material for application in millimetre-wave optical devices, during the 3D printing process [42].

In this paper, we explore the application of extensible origami structures made of high permittivity dielectric sub-units to realize a frequency tunable patch antenna. The approach is based on inserting a 3D printed dielectric origami (DO) layer in the air gap of a suspended patch and changing the configurations of the DO so as to attain a variable effective permittivity of the medium beneath the patch, and thus causing the resonant frequency of the antenna to shift. The extent of the resonant frequency shift, corresponding to the tuning range of the antenna, is determined by the variation of the geometric configuration of the DO from a fully compressed or fully dense configuration (all the faces of the elements touching each other) to a fully open configuration (elements touching only at their edges).

The organization of the paper is as follows. The fabrication of the DOs and their incorportation into the patch antenna are described in Section II. In Section III the material characterization of two DOs is presented and the effect of the DOs in their variable configurations on the resonant frequency of the patch antenna is investigated both numerically and experimentally to assess tunability. Conclusions are drawn in Section IV.

II. METHODS

Two modular origami-inspired dielectric structures were fabricated by different AM methods. The first DO consisted of a collection of right-angled triangles fabricated by FFF (Makerbot Replicator) using a bespoke filament comprising 32 vol% $BaTiO_3$ micro-powders dispersed in ABS ($\epsilon_r \sim 11$) [43]. The

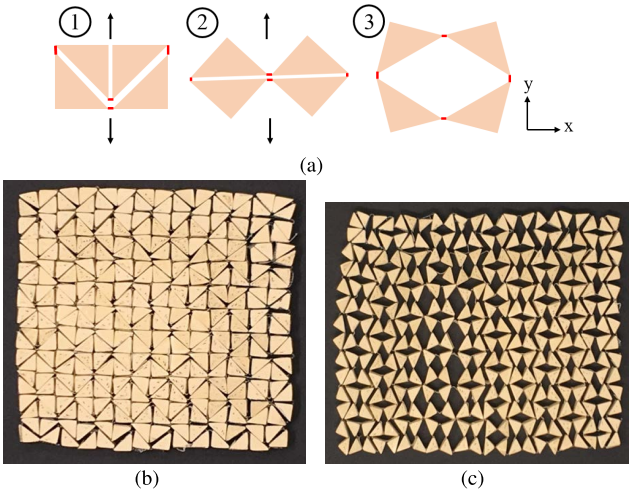

FIGURE 1. (a) The transformation of an origami unit cell from configuration 1 to 2, and 3, with arrows showing the direction of the applied force along the *y*-axis. (b) Printed $BaTiO_3$/ABS DO in its fully closed configuration and (c) in a partially expanded state.

unit cell of the DO was composed of 4 right-angled triangles with a side length of 8.5 mm and thickness of 7 mm, connected at their edges through tape, as shown in Figure 1(a) where the tape is depicted in red. By applying a force in the *y* direction, the unit cell could be transformed from the fully closed state to partially and fully expanded configurations (e.g. states 1, 2, and 3 in Figure 1(a)). The size of the whole DO assembly was 97 mm by 77 mm when fully closed or compressed, i.e., in the maximum density state, as shown in Figure 1(b). The configuration of the DO was adjusted manually. As the DO expanded as in Figure 1(c), the corresponding effective permittivity could be expected to decrease due to the progressive introduction of a greater volume fraction of air into the assembly.

To achieve a more repeatable and controllable transformation of the DO, a second DO was developed to be integrateable into a micro-linear mechanical actuation rig. The second DO consisted of a flexible lattice-like structure, printed with an elastic resin using a Formlabs 2 SLA printer, with embedded high dielectric composite triangles subsequently added by hand, which comprised 60 vol% $CaTiO_3$ micro-scale powers dispersed in ABS. The resin lattice is illustrated by the schematic drawing in Figure 2, which also shows the fabricated lattice sample. The lattice was conceived as a ''tray'' of separate triangular ''pockets'', joined at their corner edges, as detailed in Figure 2(b). The high dielectric $CaTiO_3$/ABS composite right angle triangles were placed in the pockets. The lattice had a wall thickness of 0.8 mm, and overall area of 106 mm by 114 mm. The lattice could be expanded and compressed by applying a force at its sides, thereby reconfiguring the distribution of the high permittivity elements and changing the fraction of the air voids in the assembly. Two grooves running along the two vertical sides of the lattice were used to fit rigid attachments connected to the mechanical actuator, described in Section III-C.

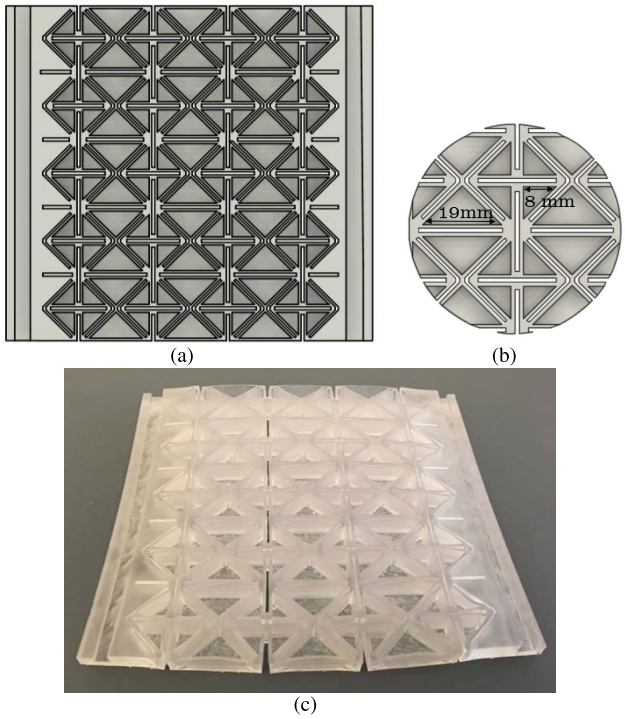

FIGURE 2. (a) CAD design of the SLA printed flexible lattice developed to reconfigure a DO in combination with a linear mechanical actuator; the grooves running on both sides are for fitting rigid handles. (b) Higher magnification view of the unit cells of the triangular structure of the flexible lattice, and (c) a photograph of the printed flexible lattice.

The high permittivity dielectric triangles were manufactured by dispersing $CaTiO_3$ power and ABS granulates in acetone until the ABS was fully dissolved. The solution was dried and the solid residue was mechanically milled into small pieces using a blade mixer. The fragments were then consolidated into a dense disc using a Dr Fritsch field assisted sintering technique (FAST) machine at 120°C and 15 MPa. The consolidated disc had a diameter of 80 mm and thickness 6.2 mm, as shown in Figure 3(a). In the FAST process, electric current is passed through a graphite die that contained the ABS-60vol%$CaTiO_3$ feedstock to provide heating, while a uniaxial pressure was exerted. The triangular dielectric elements were then obtained by sectioning the composite disc using a waterjet cutter. The two sizes of right-angle triangles were:

1) a short-side length of 8 mm, as shown in Figure 3(b),
2) a short side length of 13.5 mm.

The DO was assembled by press fitting the high permittivity dielectric triangles into the printed flexible lattice, as shown in Figure 4.

The antenna used to demonstrate our concept of frequency tunability by means of extensible origami structures was the suspended microstrip patch shown in Figure 5, where the radiating patch was printed on the bottom side of a dielectric laminate suspended in air above the antenna ground plane [44]. The DO was inserted in the air gap between the base of the antenna and the ground plane. The theoretical basis underlying the operation of this assembly is outlined in the following section.

The dielectric composite materials used for the two DOs were analysed using a JEOL JSM-6500F scanning electron microscope (SEM) to study the micro-particle distribution within the polymer matrix. For the electrical characterization of the antenna, a vector network analyzer (VNA) was used to energize the patch and to measure the reflection coefficient s_{11} at its input port. Furthermore, the effect of the different DO configurations on the suspended patch antenna were simulated extensively using CST Microwave Studio (MS) software for comparison with measurement.

A. THEORY

The resonant frequency of a suspended patch antenna can be expressed as:

$$f_r = \frac{c}{2L_{eff}\sqrt{\varepsilon_{r,eff}}} \tag{1}$$

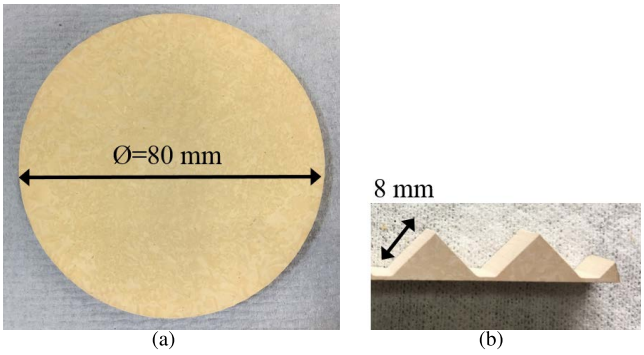

FIGURE 3. (a) Disc of $CaTiO_3$/ABS composite (diameter of 80 mm) produced by the field assisted sintering technique, and (b) triangular dielectric elements of short side length 8 mm obtained by waterjet cutting.

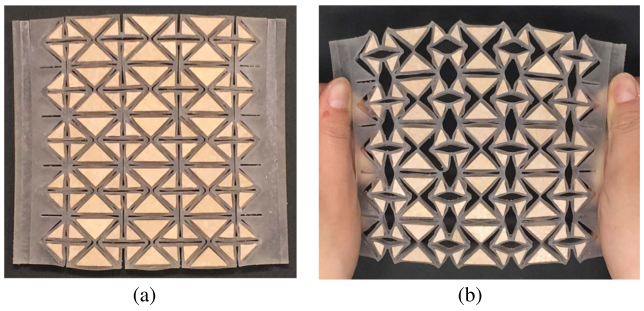

FIGURE 4. ABS-60 vol% $CaTiO_3$ DO configurations corresponding to (a) its fully compressed and (b) (manually) expanded states.

where f_r is the resonant frequency, c is the speed of light, $\epsilon_{r,eff}$ is the effective permittivity, taking into account the non-homogeneous structure of the dielectric materials, and $L_{eff} = L + 2\Delta L$ is the effective length of the patch, which because of the fringing effects, appears greater than its physical dimensions L by a distance of ΔL extended on each end. Closed form expressions for the effective permittivity and length of a microstrip patch with a multi-layered dielectric configuration have been presented in [45]. In our antenna, the square patch

was slotted with four thin rectangular cuts orthogonal to its edges to reduce the overall size of the antenna for convenience of manufacturing. This way the patch could be designed to resonate at the chosen frequency of 1 GHz, in its standalone configuration, with a side length L of 90 mm and 29.5-mm-long slots when printed on a standard 1.6-mm-thick FR4 laminate. The patch layer was suspended with an 8 mm air gap on top of a 180 mm by 180 mm ground plane made from another 1.6-mm-thick FR4 laminate. The feeding microstrip line was printed on the bottom side of the lower FR4 layer and was coupled to the patch through a rectangular slot cut at the centre of the latter. The DO sat flush on top of the ground plane and filled most of the original air gap. As a result, the antenna cross section, depicted in Figure 5(b), comprised three dielectric layers:

- the DO with adjustable configuration, and thus variable equivalent permittivity, lying on the ground plane;
- the top FR4 substrate on which the patch is printed;
- a narrow air gap between the DO and the FR4 layer of thickness $\sim$ 1 mm.

The presence of the DO in the antenna air gap modified the patch $\epsilon_{r,eff}$, and thus allows tuning the resonant frequency of the patch based on equation (1). In other words, frequency tunability could be achieved by actuating the DO into different configurations. As the antenna dimensions are fixed, both the effective permittivity and length of the patch only depend on the equivalent permittivity exhibited by the DO. Using the formulas in [45], the resonant frequency of the patch antenna can be readily estimated as a function of the permittivity of the bottom dielectric layer (ϵ_{r1}). Figure 6 illustrates this trend for a broad range of permittivity values; as the analytical expressions in [45] refer to a standard rectangular patch, without slots, an equivalent suspended patch with a larger side length of 120 mm to resonate at the same frequency of the slotted one was assumed in these calculations. It is noted that by obtaining the resonant frequency of the patch, from simulations or measurements, from the graph in Figure 6 it is possible to infer the equivalent permittivity of the DO in different configurations.

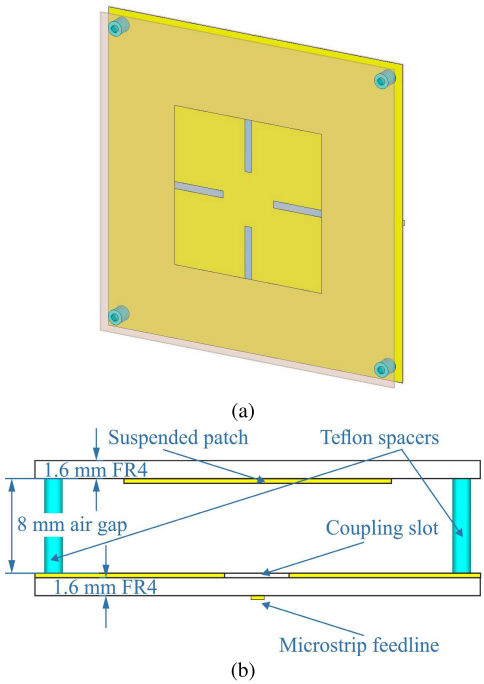

FIGURE 5. (a) Perspective and (b) cross-sectional views of the suspended patch antenna with an 8-mm-thick air gap between the ground plane and the patch. The patch side length is L = 90 mm, while the dielectric substrate is 180 × 180 mm^2. Both dielectric substrates supporting the ground plane and the patch are standard 1.6-mm-thick FR4 laminates. A rectangular slot cut at the centre of the ground plane is used to couple the patch to microstrip line running on the opposite side of the bottom FR4 substrate.

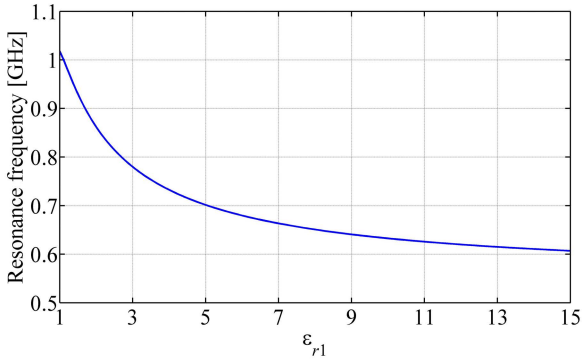

FIGURE 6. Resonant frequency of the suspended patch from Figure 5 when a dielectric layer of variable permittivity and thickness of 7 mm is inserted into the original air gap as estimated by the theoretical formulas derived in [45].

III. RESULTS AND DISCUSSION

A. MATERIAL CHARACTERIZATION

In the first DO with 30 vol% $BaTiO_3$, the composite was made into 1.75 mm diameter filament by extrusion using a 3devo single screw extruder. The composite mixture of $BaTiO_3$ micro-particles and ABS was partially melted in 160°C, and then pushed through a nozzle (2 mm). The $BaTiO_3$ particles (lighter clusters of particles) shown in Figure 7(a) were dispersed with acceptable uniformity within the ABS (darker areas). The measured permittivity of extruded ABS-30 vol% $BaTiO_3$ obtained by a QWED split post dielectric resonator (SPDR) was ϵ_r=11, with a loss tangent of 0.03. The permittivity of the dielectric composite was largely determined by the volume fraction of $BaTiO_3$. Higher ceramic fraction increases permittivity but at the cost of sacrificed flexibility and handleability, making it too brittle and unreliable for extended, reproducible 3D printing.

To explore the effect of higher ceramic loadings than those available from printable filaments, FAST was used to manufacture composite dielectric elements comprising 60 vol% $CaTiO_3$ dispersed in ABS. Figure 7(b) shows the $CaTiO_3$ particles embedded within the ABS matrix, and some small pores on the order of 1 μm. The permittivity was measured by the SPDR technique at 15 GHz as $\epsilon_r \sim$15.6 with a loss tangent of $\sim$ 0.0113.

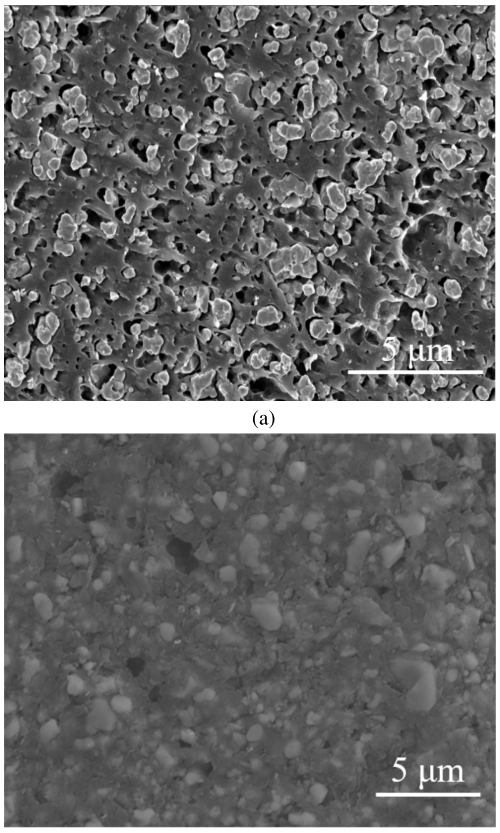

FIGURE 7. SEM images of (a) 32 vol% $BaTiO_3$ dispersed within ABS in filament form for FFF, and (b) 60 vol% $CaTiO_3$ dispersed within ABS in circular coupon form after production using FAST.

TABLE 1. Permittivity and loss tangent values for 60 vol% ceramic loading composites.

Material	ϵ_r	Loss tangent
$BaTiO_3$	18	0.0579
$CaTiO_3$	15.56	0.0113
$BaSrTiO_4$	15.56	0.0201

Other high permittivity ceramic particulates (e.g. $BaTiO_3$ and $BaSrTiO_4$) were also used to make 60 vol% loading ABS-based composites, showing the versatility of this approach, with their permittivity measured using SPDR at 15 GHz, shown in Table 1. $BaTiO_3$/ABS composite had the highest permittivity of $\sim$ 18, although $CaTiO_3$/ABS was chosen for the DO due to its relatively low loss.

B. PATCH ANTENNA WITH ABS-30VOL% $BaTiO_3$/ABS DIELECTRIC ORIGAMI

As anticipated in Section II-A, the effect of introducing a DO in the air gap of our suspended microstrip patch antenna was to modify $\epsilon_{r,eff}$ as a function of the DO configuration, thereby allowing the control of the patch resonant frequency. We consider two configurations:

i) fully compressed, which will be referred to as ''fully dense'', since in this state all the high permittivity triangles forming the DO are tightly packed and the density of the DO is at a maximum,
ii) fully actuated and the dielectric elements are inter-spaced by air voids of practically the same size, so that the density of the DO is about one half of the maximum value, referred to as ''half dense''.

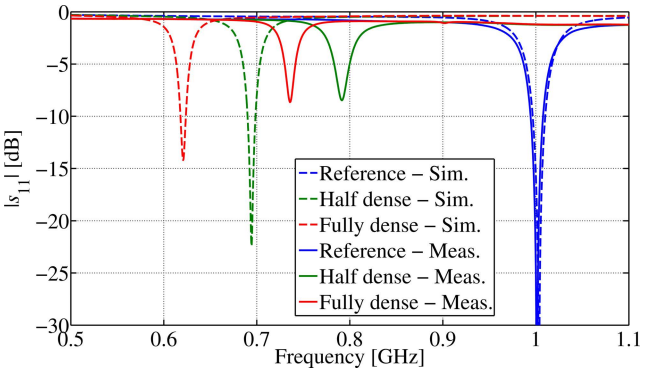

FIGURE 8. Magnitude of the reflection coefficient of the suspended patch antenna in the unloaded configuration, designed to resonate at 1 GHz, and when the composite ABS-30 vol% $BaTiO_3$ DO, in its closed and fully stretched configurations, is inserted in the antenna air gap. Experimental data (solid lines) are compared with simulation results (dotted lines).

Figure 8 shows the measured antenna reflection coefficient, s_{11}, indicating that the introduction of the fully dense DO into the air-gap layer resulted in a downward shift of the resonant frequency, from 1 GHz to 0.736 GHz. Then, by changing the DO configuration from fully dense to half dense, the antenna resonant frequency increased to 0.791 GHz, as a consequence of the lower effective permittivity. This corresponded to a maximum tunable range of 0.055 GHz, i.e., $\sim$7% with respect to the relative central frequency. A larger frequency shift was predicted by simulations, also shown in Figure 8, especially for the closed DO, giving a predictable tunability of $\sim$11%. The measured reflection coefficient s_{11} at the resonant frequency when the DO was inserted under the patch was also slightly larger than in the simulations. These inconsistencies between the simulation and experimental results might likely arise from the manual actuation of the DO and manufacturing inaccuracies, e.g. final assembly by hand. For example, stretching of the hinges connecting the elements and the resulting narrow air gaps can lead to some reduction of the effective permittivity even when in the supposedly fully dense configuration. These effects could be reduced by printing more reproducible and consistent flexible hinges that might deform more reliably during transformation, and by improving the surface finish of the DO to shrink the size of any air gap between adjacent unit cells.

The radiation pattern of the patch antenna was not expected to be significantly affected by the presence of the DO layer, according to CST MS simulations. The radiation patterns of the antenna in its reference (unloaded) configuration and when the composite ABS-30 vol% $BaTiO_3$ DO in its closed and fully stretched configurations was inserted, simulated at the respective resonant frequencies, are shown in Figure 9. The slight reduction in directivity when the antenna was

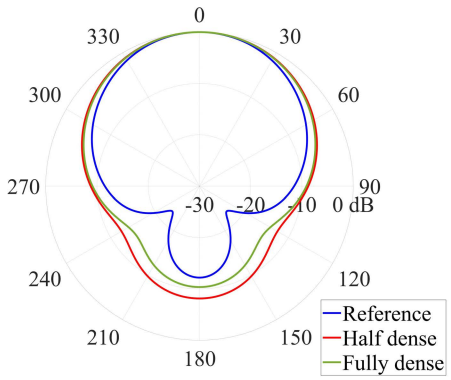

FIGURE 9. Radiation pattern of the suspended patch antenna in its reference (unloaded) configuration and when the composite ABS-30 vol% $BaTiO_3$ DO in its closed and fully stretched configurations is inserted between the patch and its ground plane as simulated with CST MS at the respective resonant frequencies.

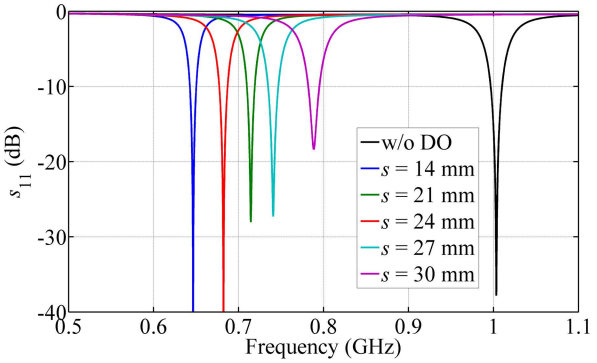

FIGURE 10. Reflection coefficients of the suspended patch when ABS-30 vol% $BaTiO_3$ DOs with unit cell of variable size (*s*) are inserted in the antenna air gap in their fully stretched configuration as simulated with CST MS.

loaded by the DO was essentially due to the smaller electrical size of the ground plane at the lower resonant frequencies. This effect could be attenuated by adopting a broader ground plane.

An insight from these results is that the range of tunability of the antenna resonant frequency might be significantly extended by tailoring the size of the DO unit cell. To investigate this, the electrical response of the patch loaded by the DO in its fully stretched configuration, which corresponds to the highest resonant frequency of the antenna for a particular DO, was simulated as a function of the size of the DO triangular constituent elements. Figure 10 shows that by choosing the size of the unit triangular elements of the DO to be 30 mm, the range of tunability of the patch resonant frequency would extend from 0.56 to 0.78 GHz, increasing the tuning range to ∼33%.

C. PATCH ANTENNA WITH ABS-60VOL%$CaTiO_3$ DIELECTRIC ORIGAMI

The mechanical actuation rig for controllable transformation of the ABS-60vol%$CaTiO_3$ DO is shown in Figure 11. Two fixtures, 3D printed using a MarkForged Onyx filament, were

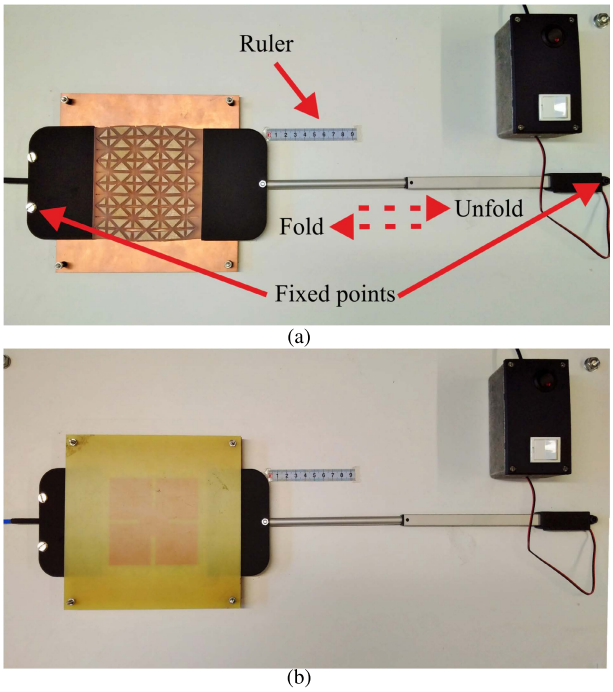

FIGURE 11. (a) Mechanical actuation rig for the ABS-30vol%$BaTiO_3$ DO. Printed Onyx fixtures are shown in black. (b) Full antenna assembly including the top dielectric substrate on which the patch is printed.

attached to the left and right hand sides of the flexible lattice; the left hand side was fixed, and the right hand side was connected to an Actuonix L16 linear actuator. A controller box was used to control the movement of the linear actuator. The linear actuator was in its fully extended state when the DO was fully closed (maximum density), and the DO then expanded as the actuator retracted. A ruler was used to measure the extension at each stage.

Using greater repeatability of the mechanical actuation, antenna reflection coefficient was measured against linear extension, up to the maximum extension of 50 mm. As the DO structure transformed upon the actuator displacement, a greater air fraction was introduced, as shown in Figure 4(b). There was a resonant frequency shift of ∼0.315 GHz for the fully closed ABS-60vol% $CaTiO_3$ DO due to its higher overall permittivity (despite some of the DO comprising the flexible lattice itself with relatively low permittivity of $\epsilon_r \simeq 3$). Correspondingly, the tuning range increased to 0.105 GHz (∼14% with respect to the central frequency), as shown in Figure 12. An estimation of the DO effective permittivity can be obtained by interpolating the plot of resonant frequency against the permittivity of the DO previously shown in Figure 6, using equation (1). The effective permittivity data are included in Figure 12 and show that, as expected, the effective permittivity of the DO progressively decreased as the structure was opened.

The effective permittivity of the DOs could be also directly estimated by homogenization theory [46]. As the continuous mechanical deformation of the DO on extension is difficult to measure accurately, the effective permittivity could only be

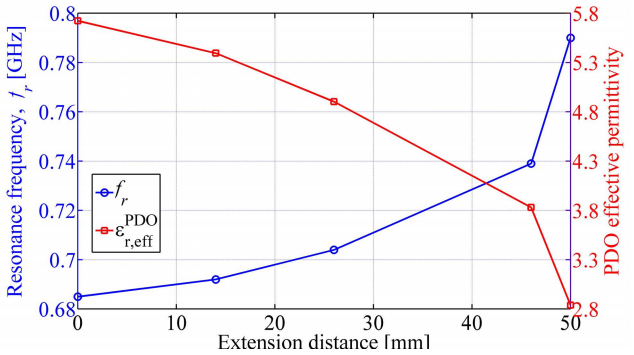

FIGURE 12. Measured resonant frequency of the suspended patch antenna against the extension distance (opening) of the ABS-60vol% $CaTiO_3$ DO (blue circles) and the corresponding estimated effective permittivity of the DO (red diamonds) as inferred from the theoretical data plotted in Figure 6.

estimated in the closed/fully compressed configuration and when fully expanded (stretched by 50 mm).

In the fully open state, the ABS-60vol% $CaTiO_3$ DO can be considered as a three components mixture: the high permittivity triangular blocks, the air voids of variable sizes between them when the structure is stretched, and the flexible resin shell. Both Maxwell Garnett (MG) [47] and the Bruggeman (Bru) [48] mixing formulas for multicomponent mixtures can be used to estimate the effective permittivity of the DO, although the latter is usually considered to yield more accurate results when the volume fraction of inclusions is not very small because of its symmetry with respect to all medium components. The Maxwell-Garnett equation for the effective permittivity of a composite medium with two different types of inclusions is given by:

$$\varepsilon_{r,eff}^{MG} = \varepsilon_{r3}\left[1+\frac{3\left(f_1\frac{\varepsilon_{r1}-\varepsilon_{r3}}{\varepsilon_{r1}+2\varepsilon_{r3}}+f_2\frac{\varepsilon_{r2}-\varepsilon_{r3}}{\varepsilon_{r2}+2\varepsilon_{r3}}\right)}{1-f_1\frac{\varepsilon_{r1}-\varepsilon_{r3}}{\varepsilon_{r1}+2\varepsilon_{r3}}-f_2\frac{\varepsilon_{r2}-\varepsilon_{r3}}{\varepsilon_{r2}+2\varepsilon_{r3}}}\right] \quad (2)$$

where for our structure $\varepsilon_{r1} = 15.6$ denotes the permittivity of the dielectric triangle blocks, and $\varepsilon_{r2} = 1$ is the permittivity of air; f_1 and f_2 are the filling fractions corresponding to the dielectric triangles and the air gaps, respectively, which we estimated to be f_1=19% and f_2=43.4%. ε_{r3}=3 is the dielectric constant of the flexible resin lattice, considered as the background of the composite structure. Bruggeman's effective permittivity for a three-components mixture is defined implicitly by the equation:

$$f_1\frac{\varepsilon_{r1}-\varepsilon_{r,eff}^{Bru}}{\varepsilon_{r1}+2\varepsilon_{r,eff}^{Bru}}+f_2\frac{\varepsilon_{r2}-\varepsilon_{r,eff}^{Bru}}{\varepsilon_{r2}+2\varepsilon_{r,eff}^{Bru}}+f_3\frac{\varepsilon_{r3}-\varepsilon_{r,eff}^{Bru}}{\varepsilon_{r3}+2\varepsilon_{r,eff}^{Bru}}=0. \quad (3)$$

where the all quantities have the same meaning as in (2) and $f_3 = 1-f_1-f_2$. Eq. (3) can be easily solved numerically.

In the fully compressed/closed configuration, the air gaps can be considered to be negligible, therefore $f_2 \sim 0$ and the above MG and Bru equations for a three-component mixture reduce to their form for a two-component medium [46]. These simplified equations only depend on f_1 (since $f_3 = 1-f_1$), which for the closed DO was $f_1 \sim 37\%$.

TABLE 2. Effective permittivities of the ABS-60vol% $CaTiO_3$ DO as estimated by Maxwell-Ganett and Bruggeman homogenization formulas when fully closed and stretched by 50 mm.

DO configuration	$\epsilon_{r,eff}^{MG}$	$\epsilon_{r,eff}^{Bru}$
Closed	5.48	6.06
50-mm-stretched	2.9	2.85

The effective permittivity of the ABS-60vol% $CaTiO_3$ DO calculated using Maxwell-Ganett and Bruggeman equations, reported in Table 2, were in good agreement for both closed and stretched (open) configurations. It is worth noting that they also agree well with Figure 12, obtained independently without taking into account the specific geometry of the DO: $\epsilon_{r,eff} \sim 5.6$ for the closed DO, and $\epsilon_{r,eff} \sim 2.8$ when the DO was stretched to 50 mm.

To assess the extent to which antenna efficiency changes at different tuning frequencies, we simulated with CST MS the effect of the DO on the antenna radiation in both the closed and fully extended configurations at the respective resonant frequencies. The directivity and gain of the unloaded microstrip patch were also simulated for reference purposes. For the Formlabs resin used to manufacture the flexible lattice, we assumed a loss tangent of 0.016 [49], while the measured dielectric properties of the high permittivity triangular blocks are those in Table 1. The results of the analyses are summarized in Table 3.

Although the introduction of the DO degraded the antenna efficiency somewhat, changes in gain as a function the resonant frequencies were relatively limited compared with, for example, frequency tunable patch antennas based on varactor diodes, especially at lower frequencies [50], [51]. The simulations also revealed that most of the losses due to the DO arose due to the presence of the flexible lattice, whose contribution to loss was comparable with the FR4 substrates used in the antenna itself. Better efficiency could therefore be achieved by making the flexible lattice with intrinsically lower loss materials with a loss tangent of $\sim 10^{-4}$, such as butyl rubber or TPE 88A, a thermoplastic elastomer available for 3D printing [52]. Estimations of the improved radiation efficiency achievable by using these materials are also included in Table 3. Another option could be to add high permittivity particulates such as $BaTiO_3$, $CaTiO_3$ or even $Bi_2(Li_{0.5}Ta_{1.5})O_7$ (permittivity ~ 64 and loss tangent $\sim 8.9 \times 10^{-5}$ [53]) into the lattice at a fraction that boosts effective permittivity while maintaining sufficient flexibility and manufacturability [54], [55].

So far in this work, we have prioritised the use of readily available materials with low cost. However, building on the current developments, a wide range of material and design optimizations immediately present themselves, since as more and more composite and other printable materials, including magnetic composites [56], become available, the DO design

TABLE 3. Directivity, gain, and the corresponding radiation efficiency of the reference patch antenna compared with those of the patch loaded by the DO when fully closed and stretched by 50 mm. Data have been simulated by CST MS for both the case of the flexible shell realized with a Formlabs resin as in our prototype and assuming alternative lower loss materials.

	Reference patch	Patch with closed origami		Patch with open origami	
Elastic shell material		**Formlabs flexible resin**	**Butyl rubber /TPE 88A**	**Formlabs flexible resin**	**Butyl rubber /TPE 88A**
Directivity (dBi)	8.4	7.34	7.3	7.35	7.27
IEEE Gain (dB)	6.8	3.89	4.91	4.61	5.16
Radiation efficiency	0.69	0.452	0.58	0.53	0.62

space becomes excitingly large. Alongside these materials developments, research in origami structures will also provide new inspiration and opportunity. For example, DO could also take the form of rotational kirigami (cut and folding) structures with shaped resonant elements. We speculate that this type of DO as an antenna substrate could be used to produce different polarization responses at different rotation angles of the sub-elements. Similarly, DO could be developed as an antenna substrate for 2D-to-2D in-plane transformations for tunable directivity and beam shaping applications.

IV. CONCLUSION

The use of modular origami-inspired dielectric layers to realize a mechanically tunable microstrip patch antenna has been investigated. The dielectric origami was designed to have an extensible and reversible metamaterial-like structure consisting of a periodic arrangement of high permittivity polymer/ceramic sub-units, linked by flexible hinges or a flexible polymer lattice. The designs were achieved using a combination of additive manufacturing, stereolithography and field assisted sintering.

Tuning of the resonant frequency of a patch antenna was achieved by placing the dielectric origami in close proximity to the antenna and then changing its geometric configuration to modify its effective relative permittivity. Actuation of the dielectric origami was achieved by hand and more controllably using a mechanical micro-linear actuator. For mechanical actuation it was necessary to embed the high permittivity composite elements into a single pre-fabricated flexible polymer lattice. This provided robust fixtures for the actuator connection, removed the variability of manually assembled hinges between elements, and allowed the full range of actuation states to be achieved reproducibly.

Experiments demonstrated tuning of the patch antenna resonant frequency by ∼14%. Increased tunability was suggested by optimizing the size of the dielectric unit cells and their permittivity, reaching a maximum tunability of ∼33%. The effective permittivity of the dielectric origami and its effect on the antenna resonant frequency was successfully estimated by homogenization theory for composite media.

The results shown here suggest that dielectric origami produced by combining advanced manufacturing techniques may provide a broad and flexible platform approach for tuning electromagnetic devices. Given the wide range of 2D and 3D origami designs available, and the many free parameters available for optimization (such as the size, shape and permittivity of dielectric elements), much greater tunability might be achieved. Further possibilities will also arise as new printable materials, including new dielectrics and magnetics become available, and new designs are discovered such as foldable and conformable structures based on origami and lattice-based kirigami elements.

ACKNOWLEDGMENT

The author Yingwei Wu thankfully acknowledges Dr. Junfu Bu for the helpful discussions and suggestions.

(Yingwei Wu and Andrea Vallecchi are co-first authors.)

REFERENCES

[1] N. Cohen, "Fractal antenna applications in wireless telecommunications," in *Proc. Prof. Program Electron. Ind. Forum New England*, May 1997, pp. 43–49.
[2] C.-Y. Pan, T.-S. Horng, W.-S. Chen, and C.-H. Huang, "Dual wideband printed monopole antenna for WLAN/WiMAX applications," *IEEE Antennas Wireless Propag. Lett.*, vol. 6, pp. 149–151, 2007.
[3] J. Liang, C. C. Chiau, X. Chen, and C. G. Parini, "Printed circular disc monopole antenna for ultra-wideband applications," *Electron. Lett.*, vol. 40, no. 20, pp. 6–7, 2004.
[4] C. G. Christodoulou, Y. Tawk, S. A. Lane, and S. R. Erwin, "Reconfigurable antennas for wireless and space applications," *Proc. IEEE*, vol. 100, no. 7, pp. 2250–2261, Jul. 2012.
[5] R. Bahr, B. Tehrani, J. Hester, J. Kimionis, and M. Tentzeris, "Additive manufacturing techniques for origami inspired 4D printed RF components and modules," in *IEEE MTT-S Int. Microw. Symp. Dig.*, Jul. 2016, pp. 1–4.
[6] A. Petosa, "An overview of tuning techniques for frequency-agile antennas," *IEEE Antennas Propag. Mag.*, vol. 54, no. 5, pp. 271–296, Oct. 2012.
[7] A. Mansoul, F. Ghanem, M. R. Hamid, and M. Trabelsi, "A selective frequency-reconfigurable antenna for cognitive radio applications," *IEEE Antennas Wireless Propag. Lett.*, vol. 13, pp. 515–518, 2014.
[8] N. Behdad and K. Sarabandi, "Dual-band reconfigurable antenna with a very wide tunability range," *IEEE Trans. Antennas Propag.*, vol. 54, no. 2, pp. 409–416, Feb. 2006.
[9] J. M. Kovitz, H. Rajagopalan, and Y. Rahmat-Samii, "Design and implementation of broadband MEMS RHCP/LHCP reconfigurable arrays using rotated E-shaped patch elements," *IEEE Trans. Antennas Propag.*, vol. 63, no. 6, pp. 2497–2507, Jun. 2015.
[10] H. Li, J. Xiong, Y. Yu, and S. He, "A simple compact reconfigurable slot antenna with a very wide tuning range," *IEEE Trans. Antennas Propag.*, vol. 58, no. 11, pp. 3725–3728, Nov. 2010.
[11] A. J. King, J. F. Patrick, N. R. Sottos, S. R. White, G. H. Huff, and J. T. Bernhard, "Microfluidically switched frequency-reconfigurable slot antennas," *IEEE Antennas Wireless Propag. Lett.*, vol. 12, pp. 828–831, 2013.
[12] L. Song, W. Gao, C. O. Chui, and Y. Rahmat-Samii, "Wideband frequency reconfigurable patch antenna with switchable slots based on liquid metal and 3-D printed microfluidics," *IEEE Trans. Antennas Propag.*, vol. 67, no. 5, pp. 2886–2895, May 2019.

[13] A.-P. Saghati, J.-S. Batra, J. Kameoka, and K. Entesari, "Miniature and reconfigurable CPW folded slot antennas employing liquid-metal capacitive loading," *IEEE Trans. Antennas Propag.*, vol. 63, no. 9, pp. 3798–3807, Sep. 2015.

[14] C. Murray and R. R. Franklin, "Frequency tunable fluidic annular slot antenna," in *Proc. IEEE Antennas Propag. Soc. Int. Symp. (APSURSI)*, Jul. 2013, pp. 386–387.

[15] C. Murray and R. R. Franklin, "Independently tunable annular slot antenna resonant frequencies using fluids," *IEEE Antennas Wireless Propag. Lett.*, vol. 13, pp. 1449–1452, 2014.

[16] H. Tang and J.-X. Chen, "Microfluidically frequency-reconfigurable microstrip patch antenna and array," *IEEE Access*, vol. 5, pp. 20470–20476, 2017.

[17] Y. Huang, L. Xing, C. Song, S. Wang, and F. Elhouni, "Liquid antennas: Past, present and future," *IEEE Open J. Antennas Propag.*, vol. 2, pp. 473–487, 2021.

[18] S. Yang, I.-S. Choi, and R. D. Kamien, "Design of super-conformable, foldable materials via fractal cuts and lattice kirigami," *MRS Bull.*, vol. 41, no. 2, pp. 130–138, Feb. 2016.

[19] G. P. T. Choi, L. H. Dudte, and L. Mahadevan, "Programming shape using kirigami tessellations," *Nature Mater.*, vol. 18, no. 9, pp. 999–1004, Sep. 2019.

[20] J. L. Silverberg, A. A. Evans, L. McLeod, R. C. Hayward, T. Hull, C. D. Santangelo, and I. Cohen, "Using origami design principles to fold reprogrammable mechanical metamaterials," *Science*, vol. 345, no. 6197, pp. 647–650, Aug. 2014.

[21] B. Treml, A. Gillman, P. Buskohl, and R. Vaia, "Origami mechanologic," *Proc. Nat. Acad. Sci. USA*, vol. 115, no. 27, pp. 6916–6921, Jul. 2018.

[22] Z. Zhai, Y. Wang, and H. Jiang, "Origami-inspired, on-demand deployable and collapsible mechanical metamaterials with tunable stiffness," *Proc. Nat. Acad. Sci. USA*, vol. 115, no. 9, pp. 2032–2037, Feb. 2018.

[23] T. Liu, Y. Wang, and K. Lee, "Three-dimensional printable origami twisted tower: Design, fabrication, and robot embodiment," *IEEE Robot. Autom. Lett.*, vol. 3, no. 1, pp. 116–123, Jan. 2018.

[24] S. Yao, X. Liu, S. V. Georgakopoulos, and M. M. Tentzeris, "A novel reconfigurable origami spring antenna," in *Proc. IEEE Antennas Propag. Soc. Int. Symp. (APSURSI)*, Jul. 2014, pp. 374–375.

[25] X. Liu, S. V. Georgakopoulos, and M. Tentzeris, "A novel mode and frequency reconfigurable origami quadrifilar helical antenna," in *Proc. IEEE 16th Annu. Wireless Microw. Technol. Conf. (WAMICON)*, Apr. 2015, pp. 1–3.

[26] S. Yao, S. V. Georgakopoulos, B. Cook, and M. Tentzeris, "A novel reconfigurable origami accordion antenna," in *IEEE MTT-S Int. Microw. Symp. Dig.*, Jun. 2014, pp. 1–4.

[27] G. J. Hayes, Y. Liu, J. Genzer, G. Lazzi, and M. D. Dickey, "Self-folding origami microstrip antennas," *IEEE Trans. Antennas Propag.*, vol. 62, no. 10, pp. 5416–5419, Oct. 2014.

[28] J. Kimionis, M. Isakov, B. S. Koh, A. Georgiadis, and M. M. Tentzeris, "3D-printed origami packaging with inkjet-printed antennas for RF harvesting sensors," *IEEE Trans. Microw. Theory Techn.*, vol. 63, no. 12, pp. 4521–4532, Dec. 2015.

[29] K. V. Wong and A. Hernandez, "A review of additive manufacturing," *ISRN Mech. Eng.*, vol. 2012, pp. 1–10, Jan. 2012.

[30] D. Espalin, J. Alberto Ramirez, F. Medina, W. M. Johnson, M. Rowell, B. Deason, M. Eubanks, B. N. Turner, R. Strong, and S. A. Gold, "Rapid prototyping journal a review of melt extrusion additive manufacturing processes: I. Process design and modeling," *Rapid Prototyping J.*, vol. 20, no. 3, pp. 192–204, 2014.

[31] S. Kumar, M. Hofmann, B. Steinmann, E. J. Foster, and C. Weder, "Reinforcement of stereolithographic resins for rapid prototyping with cellulose nanocrystals," *ACS Appl. Mater. Interfaces*, vol. 4, no. 10, pp. 5399–5407, Oct. 2012.

[32] J. A. Lewis, "Direct ink writing of 3D functional materials," *Adv. Funct. Mater.*, vol. 16, no. 17, pp. 2193–2204, 2006.

[33] C. Y. Yap, C. K. Chua, Z. L. Dong, Z. H. Liu, D. Q. Zhang, L. E. Loh, S. L. Sing, C. Y. Yap, C. K. Chua, Z. L. Dong, Z. H. Liu, D. Q. Zhang, and L. E. Loh, "Review of selective laser melting: Materials and applications," *Appl. Phys. Rev.*, vol. 2, Dec. 2015, Art. no. 041101.

[34] P. Pa, Z. Larimore, P. Parsons, and M. Mirotznik, "Multi-material additive manufacturing of embedded low-profile antennas," *Electron. Lett.*, vol. 51, no. 20, pp. 1561–1562, Oct. 2015.

[35] M. Liang, C. Shemelya, E. Macdonald, R. Wicker, and H. Xin, "3-D printed microwave patch antenna via fused deposition method and ultrasonic wire mesh embedding technique," *IEEE Antennas Wireless Propag. Lett.*, vol. 14, pp. 1346–1349, 2015.

[36] M. Altan, M. Eryildiz, B. Gumus, and Y. Kahraman, "Effects of process parameters on the quality of PLA products fabricated by fused deposition modeling (FDM): Surface roughness and tensile strength," *Mater. Test.*, vol. 60, no. 5, pp. 471–477, May 2018, doi: 10.3139/120.111178.

[37] Z. Zhao, X. Kuang, J. Wu, Q. Zhang, G. H. Paulino, H. J. Qi, and D. Fang, "3D printing of complex origami assemblages for reconfigurable structures," *Soft Matter*, vol. 14, no. 39, pp. 8051–8059, 2018.

[38] Y. Wu, A. Vallecchi, Y. Yang, Z. You, C. Stevens, E. Shamonina, and P. S. Grant, "3D printed modular origami inspired dielectrics for frequency tunable antennas," in *Proc. IEEE Int. Symp. Antennas Propag. USNC-URSI Radio Sci. Meeting*, Jul. 2019, pp. 903–904.

[39] J. Kimionis, A. Georgiadis, M. Isakov, H. J. Qi, and M. M. Tentzeris, "3D/inkjet-printed origami antennas for multi-direction RF harvesting," in *IEEE MTT-S Int. Microw. Symp. Dig.*, May 2015, pp. 1–4.

[40] W. Su, R. Bahr, S. A. Nauroze, and M. M. Tentzeris, "Novel 3D-printed 'Chinese fan' bow-tie antennas for origami/shape-changing configurations," in *Proc. IEEE Int. Symp. Antennas Propag. USNC/URSI Nat. Radio Sci. Meeting*, Jul. 2017, pp. 1245–1246.

[41] S. I. H. Shah and S. Lim, "Review on recent origami inspired antennas from microwave to terahertz regime," *Mater. Des.*, vol. 198, Jan. 2021, Art. no. 109345. [Online]. Available: https://www.sciencedirect.com/science/article/pii/S0264127520308819

[42] L. Fieber, S. S. Bukhari, Y. Wu, and P. S. Grant, "In-line measurement of the dielectric permittivity of materials during additive manufacturing and 3D data reconstruction," *Additive Manuf.*, vol. 32, Mar. 2020, Art. no. 101010. [Online]. Available: https://www.sciencedirect.com/science/article/pii/S2214860419318214

[43] Y. Wu, D. Isakov, and P. Grant, "Fabrication of composite filaments with high dielectric permittivity for fused deposition 3D printing," *Materials*, vol. 10, no. 10, p. 1218, Oct. 2017.

[44] K. F. Lee and K.-F. Tong, *Microstrip Patch Antennas*. Singapore: Springer, 2016, pp. 787–852, doi: 10.1007/978-981-4560-44-3_29.

[45] M. Biswas and M. Sen, "Design and development of rectangular patch antenna with superstrates for the application in portable wireless equipments and aircraft radome," *Microw. Opt. Technol. Lett.*, vol. 56, no. 4, pp. 883–893, Apr. 2014, doi: 10.1002/mop.28197.

[46] V. A. Markel, "Introduction to the Maxwell Garnett approximation: Tutorial," *J. Opt. Soc. Amer. A, Opt. Image Sci.*, vol. 33, no. 7, pp. 1244–1256, Jul. 2016. [Online]. Available: http://josaa.osa.org/abstract.cfm?URI=josaa-33-7-1244

[47] J. C. M. Garnett, "Colours in metal glasses and in metallic films," *Philos. Trans. Roy. Soc. London*, vol. 203, pp. 385–420, Jan. 1904. [Online]. Available: http://www.jstor.org/stable/90866

[48] D. A. G. Bruggeman, "Berechnung verschiedener physikalischer Konstanten von heterogenen Substanzen. I. Dielektrizitätskonstanten und Leitfähigkeiten der Mischkörper aus isotropen Substanzen," *Annalen der Physik*, vol. 416, no. 7, pp. 636–664, 1935, doi: 10.1002/andp.19354160705.

[49] N. Duangrit, B. Hong, A. D. Burnett, P. Akkaraekthalin, I. D. Robertson, and N. Somjit, "Terahertz dielectric property characterization of photopolymers for additive manufacturing," *IEEE Access*, vol. 7, pp. 12339–12347, 2019.

[50] S. V. Hum, "Analysis of varactor diode-tuned frequency agile antennas," in *Proc. 4th Eur. Conf. Antennas Propag.*, Apr. 2010, pp. 1–5.

[51] M. Al Ahmad, S. Kabeer, A. A. Sanad, and L. J. A. Olule, "Compact single-varactor diode frequency-reconfigurable microstrip patch antenna," *IET Microw., Antennas Propag.*, vol. 15, no. 9, pp. 1100–1107, Mar. 2021, doi: 10.1049/mia2.12117.

[52] D. Kalaš, K. Šíma, P. Kadlec, R. Polanský, R. Soukup, J. Řeboun, and A. Hamáček, "FFF 3D printing in electronic applications: Dielectric and thermal properties of selected polymers," *Polymers*, vol. 13, no. 21, p. 3702, Oct. 2021.

[53] D. Zhou, L.-X. Pang, D.-W. Wang, C. Li, B.-B. Jin, and I. M. Reaney, "High permittivity and low loss microwave dielectrics suitable for 5G resonators and low temperature co-fired ceramic architecture," *J. Mater. Chem. C*, vol. 5, no. 38, pp. 10094–10098, 2017.

[54] F. Xiang, H. Wang, and X. Yao, "Preparation and dielectric properties of bismuth-based dielectric/PTFE microwave composites," *J. Eur. Ceram. Soc.*, vol. 26, nos. 10–11, pp. 1999–2002, Jan. 2006.

[55] S. S. Kim, S. B. Jo, K. I. Gueon, K. K. Choi, J. M. Kim, and K. S. Churn, "Complex permeability and permittivity and microwave absorption of ferrite-rubber composite at X-band frequencies," *IEEE Trans. Magn.*, vol. 27, no. 6, pp. 5462–5464, Nov. 1991.
[56] Y. Wang, F. Castles, and P. S. Grant, "3D Printing of NiZn ferrite/ABS magnetic composites for electromagnetic devices," *MRS Proc.*, vol. 1788, pp. 29–35, Jul. 2015.

YINGWEI WU received the D.Phil. degree in materials from the University of Oxford, in 2021. Since October 2021, she has been a Project Leader at TWI in the laser additive manufacturing section, researching on advanced manufacturing technologies. Her research focuses on printing and designing of graded composite materials for the applications of devices that work in the microwave frequency range. She is also interested in research on utilizing different printing techniques to achieve active device tuning through various mechanisms.

ANDREA VALLECCHI (Member, IEEE) received the Laurea (M.Sc.) degree *(summa cum laude)* in electronic engineering from the University of Florence, Florence, Italy, and the Ph.D. degree in information engineering, applied electromagnetics, and telecommunications from the University of Salerno, Salerno, Italy. After completing his Ph.D. degree, he was a Research Associate with the Laboratory of Antennas and Microwaves, University of Florence. In 2008, he joined the University of Siena, Siena, Italy, as a Postdoctoral Research Fellow. From 2008 to 2010, he was a Contract Professor for the course "optical components" at the School of Engineering, University of Siena. He has been a Visiting Research Fellow at the Queen's University of Belfast, Belfast, U.K., on several occasions, and a Visiting Researcher at the University of California at Irvine, Irvine, CA, USA, in 2009. Since 2015, he has been with the Department of Engineering Science, University of Oxford, Oxford, U.K. In 2019 and 2021, he was a Tutorial Lecturer in engineering at the St. Hugh's College, University of Oxford. His research interests include the theoretical modeling and design of metamaterials, metasurfaces, and metamaterial-inspired antennas for applications at microwaves, THz, and optical frequencies. He was a co-recipient of the "Best Antenna Theory Paper Award" at the 8th European Conference on Antennas and Propagation in 2014. He received an "Excellence Award for Outstanding Performance Throughout 2019" from the Department of Engineering Science, University of Oxford. In 2013, he was awarded a Marie Curie Research Fellowship at The University of Sheffield, Sheffield, U.K.

YUNFANG YANG received the bachelor's degree from Tsinghua University, where she had a background in soft robotics and bio-printing. She is currently a Postdoctoral Researcher in engineering science at the University of Oxford. She is also a Clarendon Scholar with the University of Oxford, aiming to combine her knowledge in mechanism design with computational fabrication for smart active materials in the future. Her research involves using origami/kirigami mechanisms to design reconfigurable materials with interesting properties and performance. The materials she designs can change their shape, density, and elastic energy through transformation, which provide a variety of potential application, from multifunctional metamaterials, soft robotics, to kinetic architecture.

ZHONG YOU is currently a Professor of engineering science at the University of Oxford. His research interests include deployable structures and origami structures, both of which are capable of large shape change. One of the highlights of his work is the development of a systematic approach to create large deployable structures using known mechanisms based on mathematical tiling and patterns.

EKATERINA SHAMONINA (Member, IEEE) received the degree in physics from Moscow State University, and the Ph.D. and Habilitation degrees in theoretical physics from the University of Osnabrueck, Germany. She is currently a Professor of engineering science at the University of Oxford. She is also the Head of OxiMeta, Oxford Metamaterials Centre. She is a Co-Founder and the Director of a university spinout company Metaboards Ltd., developing metamaterial-based advanced wireless power and data technologies. Her main research interests include metamaterials, amorphous semiconductors, photorefractive materials, antennas, and plasmonics.

CHRISTOPHER J. STEVENS (Member, IEEE) received the Graduate degree (Hons.) in physics from the University of Oxford, Oxford, U.K., in 1990, and the D.Phil. degree in condensed matter physics, in 1994, following a three-year Ph.D. degree course at the University of Oxford. He worked with the Uiversita Degli Studidi Lecce on the properties of wide band gap semiconductor materials. He was a Postdoctoral Fellow with the Clarendon Laboratory on the dynamic properties of high temperature superconductors, after which he held a Royal Academy of Engineering Fellowship at the St. Hugh's College, Oxford. During this period, he developed a number of novel devices based on kinetic inductance and photomixing effects. He is currently an Associate Professor of engineering science at the University of Oxford. His current research interests include ultrawideband communications, metamaterials, ultrafast nanoelectronics, and high-speed electromagnetics. He is also a fellow of the St. Hughs College. He received awards for practical physics.

PATRICK S. GRANT is currently a Vesuvius Chair of materials and a Pro-Vice-Chancellor for research at the University of Oxford. His research concerns developing and understanding novel methods of materials manufacture, especially the evolution of structure across a range of length-scales. His current work focuses on the manufacture of smart supercapacitors and Li ion battery electrodes, three-dimensional printing of multi-materials for microwave applications, and new alloys and processes for materials recirculation. He is a fellow of the Royal Academy of Engineering.